CrossMark

Thermal and spectroscopic (IR, XPS) properties of lanthanide(III) benzene-1,3,5-triacetate complexes

Justyna Sienkiewicz-Gromiuk[1] · Iwona Rusinek[1] · Łukasz Kurach[2] ·
Zofia Rzączyńska[1]

Abstract The metal–organic frameworks of the formula Ln(bta)·nH$_2$O where $n = 3, 4, 5$ or 6; bta = benzene-1,3,5-triacetate ion: $[C_9H_9(COO)_3]^{3-}$; Ln = La(III), Nd(III), Eu(III), Tb(III), Ho(III), Tm(III), Lu(III) were synthesized by the reaction of LnCl$_3$·xH$_2$O with ammonium salt of H$_3$bta acid in water solution. Insoluble water compounds crystallize in the monoclinic or triclinic crystal system, and they are stable up to 30 °C. When heated, they decompose up to 160–200 °C in two stages to stable anhydrous compounds. The dehydrated compounds Ln(bta) are still crystalline and stable up to about 350 °C. When heated above 350 °C, they undergo decomposition where the intermediate products are Ln$_2$O$_2$CO$_3$ or Tb$_4$O$_6$CO$_3$ and the residues are: Ln$_2$O$_3$ or Tb$_4$O$_7$. The interpretation of IR spectra of title compounds was made taking into consideration the experimental and theoretical wavenumbers obtained for H$_3$bta specie. The XPS spectra of H$_3$bta and its complexes were recorded. The way of metal–carboxylate group of ligand coordination was discussed. This work presents the results of the XPS analyses, which allowed to determine the binding energies (E_b) for the main lines of Ln3d, Ln4d, Ln5p, C1s, O1s spectra, spin–orbital splitting and full width at half maximum complexes.

Introduction

The field of inorganic open-framework materials is dominated by aminosilicates and phosphates, but metal coordination polymers based on organic ligands have emerged as an important family in the last two decades. These metal–organic frameworks (MOFs) are a class of crystalline hybrid materials in which metal ions in the solid structure are linked by various organic bridging ligands. As the bridging ligands in the MOF structures, there are used O- and N-donor ligands, but coordination centres are transition metal as well as lanthanide(III) ions [1, 2]. In that family of materials, the metal carboxylates are specially interesting since they contain both organic and inorganic components: they not only form open-framework structures resulting from the presence of the carboxylate function itself, but also where the carboxylate group acts as a linker between inorganic moieties. Lanthanide(III) carboxylates attract the attention because of their luminescence properties and their spectrally narrow emission [3–6]. The large magnetic moment of the most of the lanthanide(III) ions together with their anisotropy makes these ions very useful in preparation of magnetic materials [7, 8]. The compounds become interesting also in searching for promising application in drug delivery, gas absorption as well as separation and catalysis [9, 10].

Benzene multicarboxylate ligands are frequently applied in the construction of lanthanide(III) polymeric 1D, 2D and higher-dimensional frameworks. The exemplary compounds are lanthanide benzenedicarboxylates [11], benzene-1,3,5-tricarboxylates [12], benzene-1,2,4,5-tetracarboxylates [13]

✉ Zofia Rzączyńska
z.rzaczynska@poczta.umcs.lublin.pl

[1] Department of General and Coordination Chemistry, Faculty of Chemistry, Maria Curie-Sklodowska University, M.C. Sklodowska Sq. 2, 20-031 Lublin, Poland

[2] Department of Synthesis and Chemical Technology of Pharmaceutical Substances, Medical University of Lublin, Chodźki 4A, 20-093 Lublin, Poland

and benzene-1,2,3,4,5,6-hexacarboxylates [14]. In each of the series of lanthanide complexes, one can observe two or three isostructural series indicating that the decreasing lanthanide ion radius has influence on the complex structure.

Recently, some interest has arisen in the construction of lanthanide MOFs with flexible organic ligands for example: Tb(III) and Ho(III) phenylene-1,2-diacetates [15], Sm(III), Eu(III), Tb(III), Ho(III) phenylene-1,3-diacetates [16], lanthanide phenylene-1,4-diacetates [17] and benzene-1,3,5-triacetates (Scheme 1) [18–21] owing to their flexibility and conformational freedoms. The use of lanthanide ions in that construction is due to the high coordination number (8 or 9) as well as special properties of the lanthanide ions.

This paper describes the synthesis, structural and thermal characterization of selected lanthanide complexes with the flexible bta ligand. Taking into consideration the high but changing coordination number of Ln^{3+} ions, reducing of their radius, diversity of carboxylate group-Ln^{3+} binding mode [22] as well as the flexible character of bta ligand [23] which can adopt different conformations in the

process of MOFs formation proceeded under the stable conditions of synthesis. The conditions of synthesis have great impact on the structure of MOFs [20]. The aim of this paper was also to determine the influence of temperature increase on the stability of crystalline networks of the complexes. Net water molecules in the complex structure should be easily removed from the outer- and inner- coordination spheres without the lanthanide–organic framework collapse. In this way, the coordinatively unsaturated lanthanide ions can cause catalytic or surface activity of the porous complex materials. This inspires the research groups to seek the porous lanthanide–organic frameworks (MOFs).

Experimental

Preparation of the lanthanide(III) complexes

The flexible bta ligand is versatile and can adopt different conformations in the formation of complexes so conditions
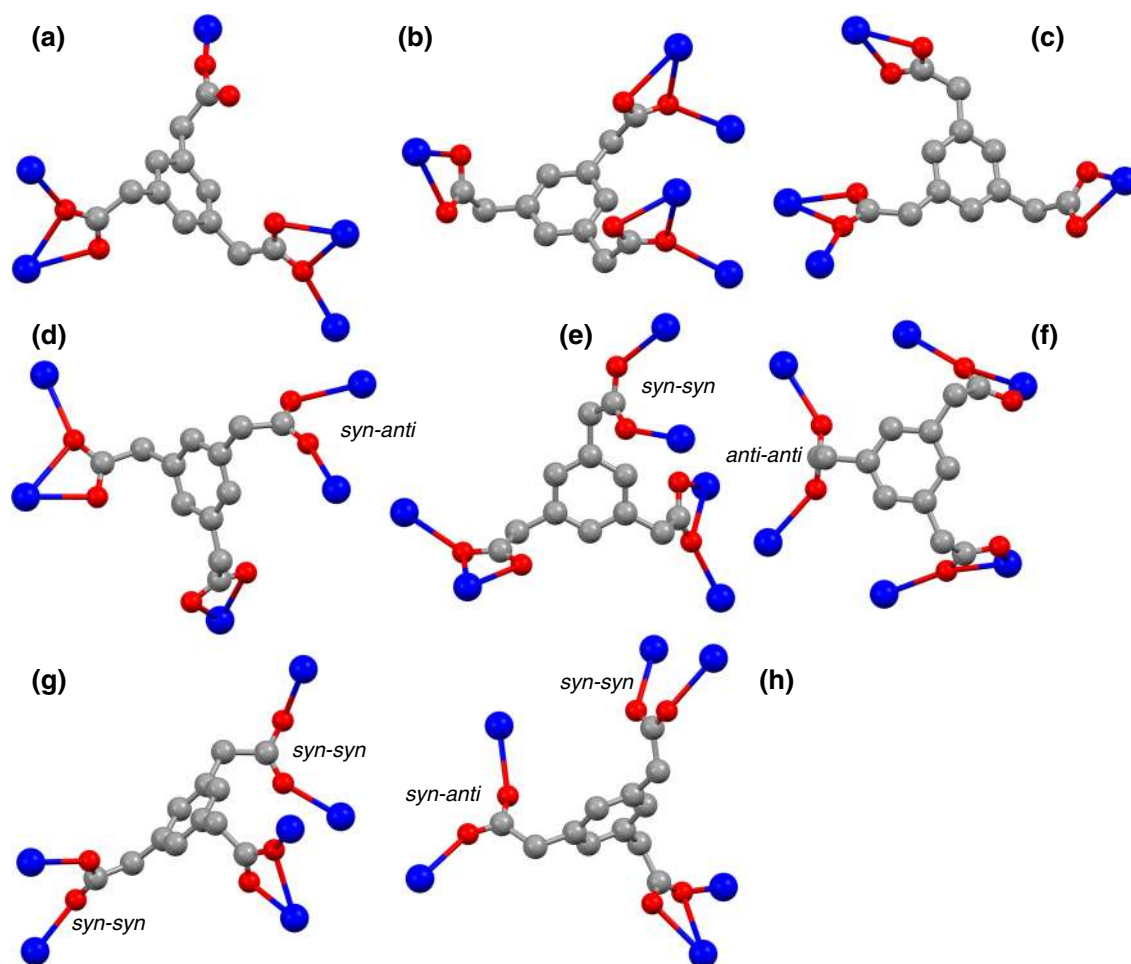
Scheme 1 Possible coordination modes of bta ligand in the lanthanide(III) complexes [18–21]

of reaction have a great impact on the MOFs structure [20]. The whole series of lanthanide(III) complexes was prepared under exactly the same conditions: in the reaction of lanthanide(III) chlorides (pH 5.3–5.8) and the ammonium salt of H_3bta (pH $\approx$ 5.5) in the 0.01 M solutions at 40 °C at the molar ratio 1:1. The $LnCl_3$ solutions were obtained in the reactions of appropriate rare earth oxides with 2 M solution of HCl. Next, these $LnCl_3$ solutions reacted with a soluble form of the ligand, which was ammonium salt $bta(NH_4)_3$. The precipitates were filtered, washed with hot water to remove NH_4^+ ions and dried at 30 °C to the stable mass. The complexes were identified by the method of elemental analysis, and the lanthanide contents were determined on the basis of the registered TG curves from the thermogravimetric analyses. The results of elemental analysis for the obtained complexes are gathered in Table 1.

Physical techniques

The complexes were identified by the method of elemental analysis with a CHN 2400 Perkin–Elmer analyser. The contents of metal ions were determined on the basis of the registered TG curves from the thermogravimetric analyses. The IR spectra of the compounds were recorded over the range 4000–400 cm^{-1} using a IR SPECORD M80 spectrophotometer. The thermal behaviour of the compounds was investigated by a Setsys 16/18 Setaram thermoanalyser, registering TG, DTG and DSC curves. The samples (7–8 mg) were heated in the ceramic crucible in the temperature range 30–1000 °C in the flowing air atmosphere (1 dm^3 h^{-1}) with the heating rate 10 °C min^{-1}. Gaseous products of decomposition of Tb(III) complex were identified using a Netzsch TG 209 apparatus coupled to a Bruker FTIR 66 spectrophotometer. The samples were heated in the dynamic argon atmosphere with a rate of 20 °C min^{-1} up to 1000 °C using a ceramic crucible.

For studied complexes, there were conducted powder X-ray diffraction experiments (XRPD) at 30, 250 and

800 °C using a PANalytical Empyrean automated X-ray diffractometer with the XRK-900 RIGID high-temperature reaction chamber. Cu Kα radiation ($\lambda = 1.54187$ Å) was used for the diffraction experiments conducted in the non-continuous scanning mode. The first scan was at 30 °C; then, the sample was heated with the rate of 60 °C min^{-1} up to 250 °C and stabilized for 5 min and scanned using the goniometer in the theta–theta orientation, next heated up to 600 °C, stabilized again for 5 min and scanned and finally up to 800 °C in the same way. The samples were dried, fine-powdered and applied to a low-background sample holder. In a typical experiment, data were collected via continuous scan in the range of $2\theta = 5$–90° with the step size of 0.02626° and a scan time of 180 s per step.

The X-ray photoelectron spectra (XPS) were measured on a UHV Prevac spectrometer. Monochromatic Al Kα radiation (1486.6 eV) was used from an X-ray gun operated at 12 kV and 30 mA. The powder samples were pressed into pellets, and then, they were transferred via a sample probe in the electron energy analyser chamber which had a base pressure in the range of 10^{-11} mbar in the analyser. For all samples, the intense carbon 1s photopeak of aromatic hydrocarbon character in the compounds was used as a standard for the binding energy. The binding energy at the standard peak was determined to be 284.8 eV.

Computational details

The molecular structure optimization of the H_3bta and corresponding vibrational harmonic frequencies were calculated using the DFT with B3LYP combined with 6-311++G(d,p) basis set using Gaussian 03 W program package [24]. The starting atomic coordinates were taken from the crystal structure of the H_3bta (Scheme 2) determined from X-ray crystallography [23]. The absence of imaginary wavenumbers of the calculated vibrational spectrum confirms that the optimized structure of H_3bta is stable. In order to get better correlation between the calculated and the experimental frequencies, the calculated vibrational frequencies were scaled by two different scaling factors, i.e. 0.983 up to 1700 cm^{-1} and 0.958 for greater than 1700 cm^{-1} [25]. The assignments of the calculated wavenumbers were examined by means of PEDs using VEDA 4 program [26].

Results and discussion

Thermal analysis

Thermogravimetric analyses (TG) were performed for dried, powdered, crystalline samples of the complexes in

Table 1 Elemental analysis data of benzene-1,3,5-triacetates obtained under conventional conditions

Complex	C/%		H/%		Ln/%	
	Found	Calcd	Found	Calcd	Found	Calcd
La(bta)·6H$_2$O	29.85	30.11	4.15	3.97	27.02	27.99
Nd(bta)·4H$_2$O	30.76	30.93	3.60	3.65	31.30	30.99
Eu(bta)·4H$_2$O	30.41	30.43	3.57	3.59	32.30	32.11
Tb(bta)·4H$_2$O	29.84	29.99	3.46	3.54	32.88	33.10
Ho(bta)·4H$_2$O	29.46	29.62	3.44	3.49	33.11	33.92
Tm(bta)·5H$_2$O	28.37	28.33	3.85	3.73	33.73	33.24
Lu(bta)·3H$_2$O	27.07	27.96	3.74	3.69	36.90	37.19
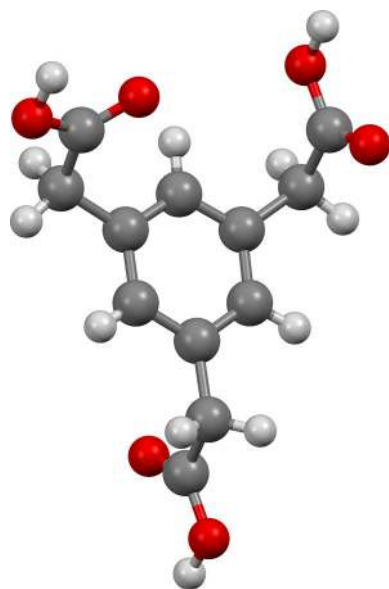
Scheme 2 Molecular structure of neutral H_3bta [23]

Fig. 2 TG and DTG curve of Tb(III) complex in argon

the range of 30–1000 °C under air as well as argon atmosphere. The TG data show that complexes of the general formula $LnC_9H_9(COO)_3 \cdot 3–6H_2O$, where Ln = La(III), Nd(III), Eu(III), Tb(III), Ho(III), Tm(III), Lu(III) heated in air (Fig. 1) as well as argon atmosphere (Fig. 2), are stable up to 30 °C, and then, the dehydration process takes place.

The TG and DSC curves show two steps of dehydration which means that in the structure of complexes there are hydrogen- and coordination-bonded water molecules.

Determination of the number of water molecules in the outer- and inner- coordination spheres of compounds on the basis of TG and DSC analysis is sometimes possible, but in majority of cases removing hydrogen-bonded water causes
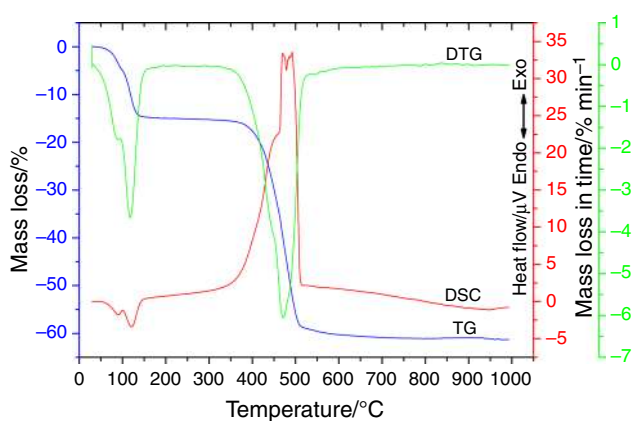

Fig. 1 TG, DTG and DSC curves of thermal decomposition of Tb(bta)$\cdot$4H$_2$O in air
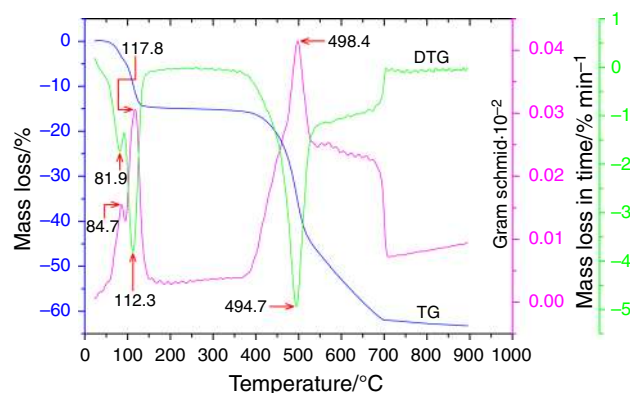
total dehydration in one stage as it is in the case of La(III) complex. Neither on TG, DTG nor DSC curves, two peaks are observed although the complex contains two types of differently bonded water molecules. In the case of the other complexes, hydrogen-bonded water molecules are disconnected in the first step at lower temperatures: 110, 100, 90, 80, 100, 95 °C for Nd(III), Eu(III), Tb(III), Ho(III), Tm(III) and Lu(III) complexes, respectively, and then, the molecules of coordinated water are released at about 145, 130, 126, 120, 145 and 140 °C for Nd(III) and successive compounds. This two-step dehydration process is clearly visible for example on the TG, DTG and DSC curves for the Tb(III) complex in air (Fig. 1), in argon (Fig. 2) as well as on the IR spectra of gaseous products of decomposition at 90 and 126 °C (Fig. 3). The process of involving the water molecules observed on the TG curves is characterized by total mass loss in the range 10.63–21.82 % (Table 2). The values of dehydration energy calculated from the DSC curves are the sum of the enthalpy of disconnection of hydrogen- and coordination-bonded water molecules. These values increase with the increasing atomic number of Ln(III) ions, but generally the total energy of dehydration is in the range 28.55–35.78 kJ mol^{-1} H$_2$O in the complexes.

After dehydration, the anhydrous compounds are stable up to about 300–350 °C. Further heating leads to the degradation of anhydrous compounds, which is accompanied by burning of organic ligand. The final products of decomposition are suitable lanthanide oxides.

The simultaneous FT-IR analysis of gaseous products of thermal decomposition was made for Tb(bta)$\cdot$4H$_2$O complex (Fig. 3). The results obtained from TG-FT-IR measurement confirm that the first loss of mass observed in the temperature range 30–98 °C is connected only with the removal of outer-sphere water molecules. Figure 3 shows the separated spectra of valence and deformation vibration of water molecules at 3750 and 1750 and 1900–1300 cm^{-1}
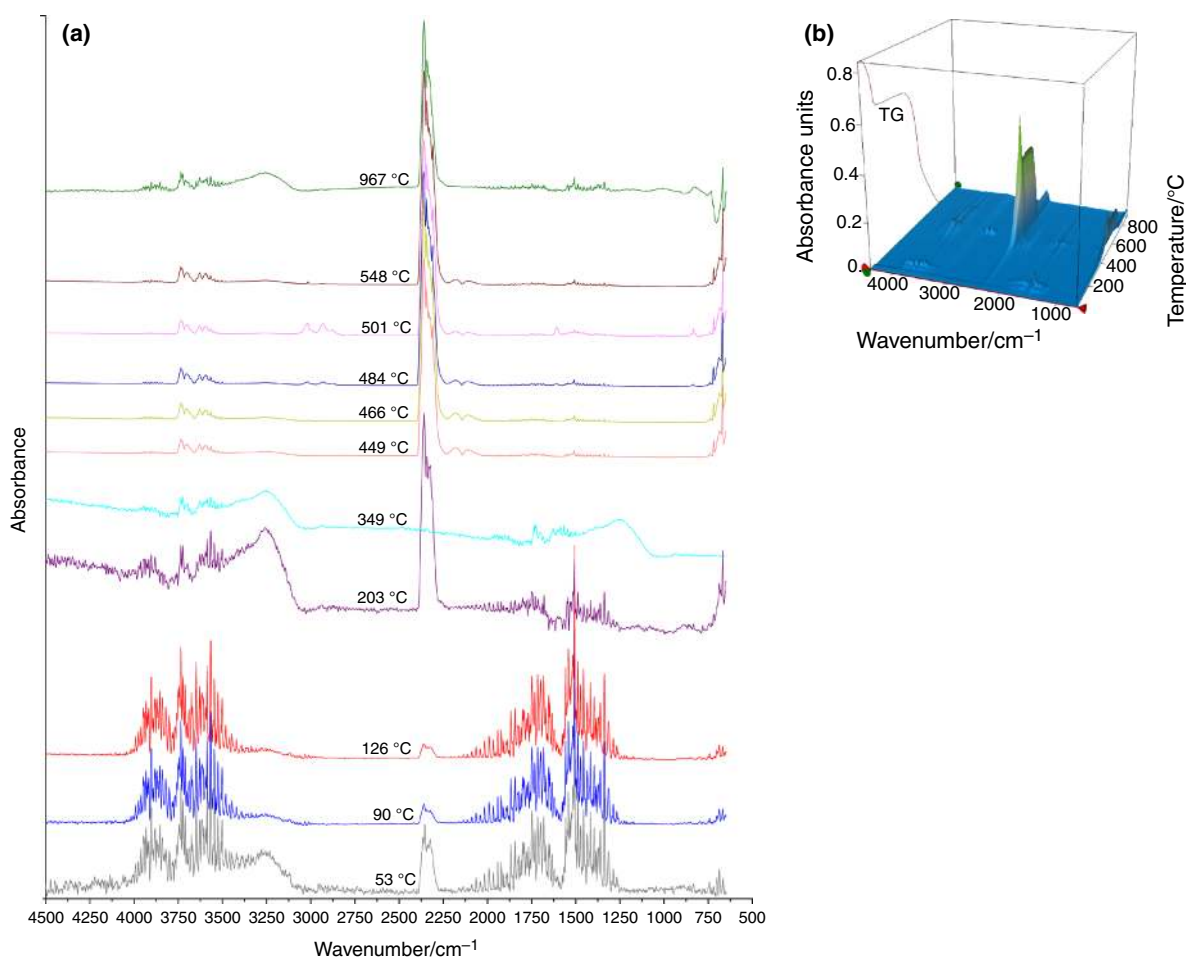
Fig. 3 Line plot of FT-IR spectra of the evolved gases for Tb(bta)·4H$_2$O (**a**); three-dimensional FT-IR spectra of gaseous products of thermal decomposition of Tb(bta)·4H$_2$O (**b**) in argon

Table 2 Results of thermal analysis of lanthanide(III) benzene-1,3,5-triacetates

Compound	M_{mol}	ΔT_1/°C	Mass loss/%		Endothermic effect/(kJ mol^{-1})	T_2/°C	Residue/%	
			Calcd	Found			Calcd	Found
La(bta)·6H$_2$O	496.12	30–180	21.76	21.82	28.55	330	32.83	31.70
Nd(bta)·4H$_2$O	465.46	30–200	15.46	15.56	29.13	340	36.13	36.51
Eu(bta)·4H$_2$O	473.18	30–160	15.21	14.81	35.78	300	37.19	37.41
Tb(bta)·4H$_2$O	480.15	30–160	14.99	14.95	35.53	350	38.92	38.67
Ho(bta)·4H$_2$O	486.15	30–160	14.81	14.74	33.46	330	38.85	34.15
Tm(bta)·5H$_2$O	508.15	30–180	17.71	18.27	31.94	350	37.96	38.52
Lu(bta)·3H$_2$O	478.19	30–180	11.29	10.63	32.39	350	41.61	42.30

ΔT_1, temperature range of dehydration process; T_2, temperature at the start of decomposition

[27], and the second part of water spectra appearing at the higher temperature, about 126 °C belonging to coordination water. Formation of the stable, anhydrous compound is confirmed by the lack of bands in the existing anhydrous, stable complex in the temperature range 130–300 °C. During further decomposition of the complex at higher temperatures CO$_2$, CO and hydrocarbons are released. The carbon dioxide bands showed strong absorption peaks of

Table 3 Unit cell parameters for polycrystalline lanthanide(III) benzene-1,3,5-triacetates

Crystal system	Complex				
	Nd(bta)·4H$_2$O Triclinic	Eu(bta)·4H$_2$O Triclinic	Tb(bta)·4H$_2$O Triclinic	Ho(bta)·4H$_2$O Triclinic	Lu(bta)·3H$_2$O Monoclinic
a/Å	7.3036	7.2774	7.2755	7.2707	10.1956
b/Å	10.8993	10.8011	10.8033	10.7761	12.0537
c/Å	11.1349	11.0948	11.0976	11.1072	14.4138
α/°	62.829	62.692	62.551	62.472	90.00
β/°	77.798	77.733	77.539	77.453	100.216
γ/°	80.224	80.186	80.060	80.011	90.00
V/Å^3	768.02	754.53	753.14	750.60	1743.30
M_{20}	20.3	13.3	18.9	23.7	19.4
F_{20}	44.3 (0.0100, 45)	28.9 (0.0147, 47)	38.9 (0.0109, 47)	50.0 (0.0097, 41)	48.0 (0.0077, 54)
F_{N}	F_{48} = 15.0 (0.0106, 301)	F_{36} = 10.4 (0.0144, 242)	F_{42} = 15.3 (0.0132, 208)	F_{40} = 20.8 (0.0113, 170)	F_{35} = 15.4 (0.0090, 253)

N number of indexed peaks

stretching vibration at 2361 and 2330 cm^{-1} and the weak deformation peaks at 720 and 670 cm^{-1}. The bands at 2180 and 2114 cm^{-1} belong to CO molecules. The stretching absorption bands at 2900 and 2800 cm^{-1}, deformation mode at 1460 cm^{-1} and rocking vibration bands at 800 cm^{-1} appear due to the presence of hydrocarbons in the gaseous product of fragments of organic ligand decomposition [28].

The thermal stability of dehydrated complexes increases with the increasing atomic number of lanthanides, that is with the decreasing ionic radius of lanthanides. Ln$_2$O$_3$ and Tb$_4$O$_7$ are formed as the final products of decomposition.

XRD studies

Bta is a flexible ligand on account of sp^3 carbon atoms (–CH$_2$–) linking benzene as a central part of ligand with the carboxylic groups in the molecule [23]. Thus, this can cause that the series of complexes is entirely isostructural, in spite of significant differences in the size of the trivalent lanthanide ions, similar to phenylene-1,4-diacetates of lanthanides [17]. In the complexes, the lanthanide(III) ions are connected through oxygen atoms of carboxylate groups of organic ligand creating chains of metal ions. Part of water molecules completes the coordination number of lanthanide(III) ions to 9 for light and to 8 for heavy ones. Part of them is hydrogen bonded inside the complex structure. The analysed complexes crystallize in the triclinic or monoclinic crystal system (Table 3). As follows from the X-ray powder diffraction patterns (Fig. 4), the tetrahydrated ones are isomorphous. To examine stability of the crystalline frameworks of the complexes after removal of water molecules, the powder diffraction

patterns of the compounds in situ at 30, 250 and 800 °C were recorded. As follows from the comparison of the diffractograms (Fig. 5), the same system of peaks is observed at 30 and 250 °C. This indicates that the framework and crystalline order are maintained despite removal of the water molecules [29]. The high stability of the anhydrous complexes frameworks is also reflected on the TG curves (Figs. 1, 2). The anhydrous compounds heated above 300–350 °C undergo decomposition where the intermediate products are Ln$_2$O$_2$CO$_3$ and the residues are: Ln$_2$O$_3$ or Tb$_4$O$_7$ [30–33]. The above-mentioned final thermal decomposition products are confirmed by the data included in ICDD.

Infrared analysis

The infrared spectra of H$_3$bta, its sodium salt and lanthanide(III) complexes were recorded, and assignments of bands occurring in the experimental as well as calculated spectra are gathered in Table 4. The exemplary experimental IR spectra of acid, its sodium salt and the Tb(III) and Ho(III) complexes are presented in Fig. 6. Comparing the IR spectra of acid and its metal compounds, one can observe that some bands characteristic of acid spectra disappeared in the spectra of sodium and lanthanide complexes. The stretching vibration bands of v(OH) of –COOH groups exist as the broad band at 3500–2500 cm^{-1} in spite of hydrogen bonding in the acid structure. During complex formation, the strength of hydrogen bonding decreases and these bands are shifted to higher frequencies 3700–2700 cm^{-1}. The v(OH) band in the theoretical spectrum of acid is located at 3600 cm^{-1} (Table 4). The stretching asymmetric v_{as}(CH$_2$) mode of methylene groups

Fig. 4 X-ray powder diffraction patterns of polycrystalline lanthanide(III) complexes
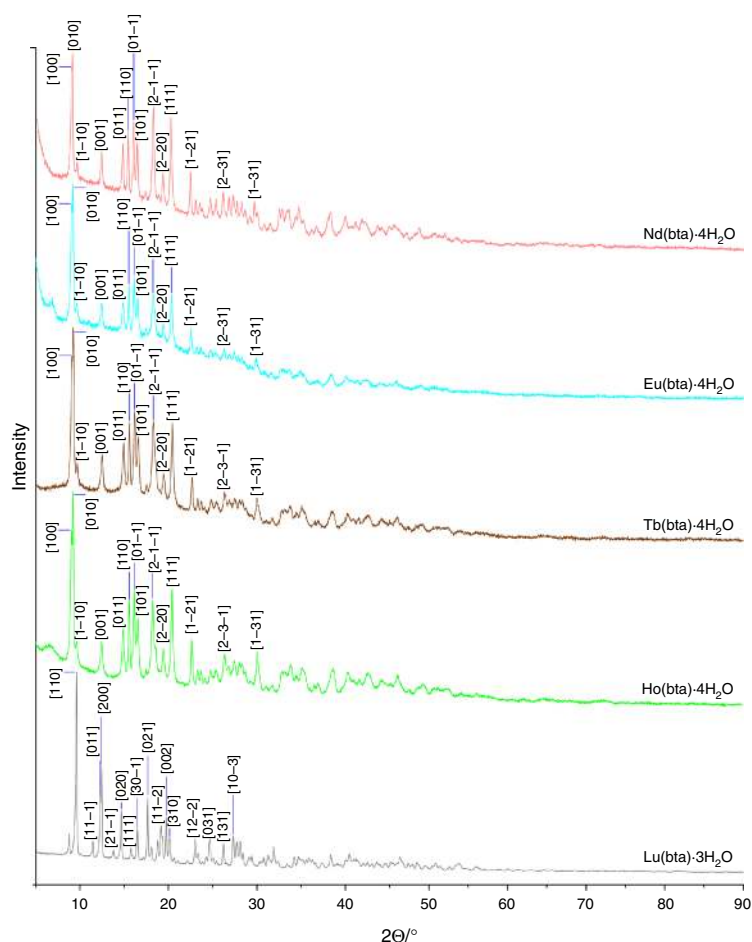

is observed in the experimental spectra at 2972, 2948 and 2970–2920 cm^{-1} at acid, sodium salt and Ln(III) complexes, but stretching symmetric $v_s(CH_2)$ vibrations are found at 2924, 2912 and 2920–2896 cm^{-1}, respectively. The calculated values for these bonding vibrations are close to the experimental data, and they are within 2992–2905 cm^{-1}. The deformation bands of scissoring vibrations $\delta(CH_2)$ appear at 1385 cm^{-1} at acid (calcd. 1457, 1436 and 1435 cm^{-1}), 1412 cm^{-1} at sodium salt and in the range of 1436–1416 cm^{-1} for the complexes; wagging mode $\omega(CH_2)$ is located at 1266 cm^{-1} in the acid spectrum (calcd. 1287 cm^{-1}), 1256 and 1272–1248 cm^{-1} for sodium and Ln(III) compounds. The twisting $t(CH_2)$ vibrations of methylene groups are seen at 1193 cm^{-1} for acid (calcd. 1194 and 1187 cm^{-1}) at 1200, 1192 and 1192–1188 cm^{-1} for sodium and Ln(III) compounds, respectively. These bands do not shift due to complex formation because this part of ligand takes place neither in the metal coordination nor hydrogen bonding formation.

The carboxylic groups are the main groups in the structure of H$_3$bta, which undergo transformation during deprotonation and metal complexes formation. The vibrational bands of carboxylic groups of acid contain the C=O, C–O and O–H vibration modes. The bands assigned to the stretching vibrations $v(C=O)$ of carboxylic group of acid molecule which usually appear about 1700 cm^{-1} in this acid appear as three strong peaks at 1723; 1705 and 1693 cm^{-1} (calcd. values 1743; 1741; 1733 cm^{-1}) (Table 4; Fig. 6) due to small difference in the lengths of C=O bonds which depends on their environment in the acid structure. These peaks disappear in sodium salt and lanthanide complexes due to complete deprotonation of each carboxylic group and metal compound formation. So new, very strong bands assigned to the asymmetric $v_{as}(COO^-)$ and symmetric $v_s(COO^-)$ stretching vibrations of carboxylate anion appear. The asymmetric and symmetric bands of carboxylate group vibrations in sodium salt are located at 1580 and 1384 cm^{-1}, whereas in the lanthanide complexes they are situated in the region of 1564–1536 and 1436–1396 cm^{-1} as presented in Fig. 6 and Tables 4 and 5. In all registered IR spectra of lanthanide(III) compounds, each absorption band of stretching symmetric carboxylate $v_s(COO^-)$ vibrations is split, which indicates the presence of more than one coordination mode of carboxylate groups

Fig. 5 X-ray powder diffraction patterns of polycrystalline Ho(bta)·4H$_2$O (30 °C), Ho(bta) (250 °C) and Ho$_2$O$_3$ (800 °C)
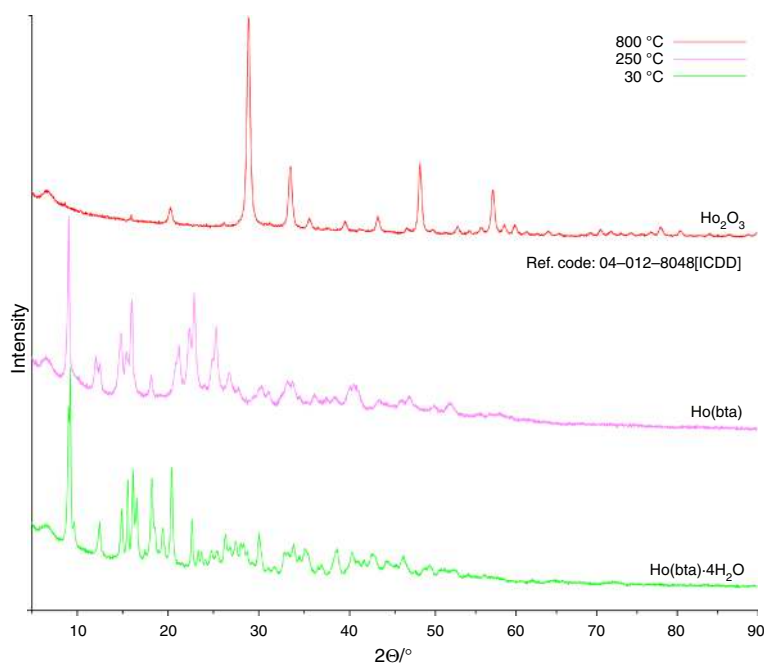
of bta ligand. On the basis of the difference Δv between the wavenumbers $v_{as}(COO^-)$ and $v_s(COO^-)$ of carboxylate anion, the type of coordination of –COO$^-$ group by metal ions in the studied complexes can be analysed. According to the Nakamoto spectroscopic criterion [34], mode of carboxylate binding can be ionic, monodentate, bidentate chelating or bridging according to the series: Δv chelating $< \Delta v$ bridging $< \Delta v$ ionic $< \Delta v$ monodentate. The $\Delta v(COO^-)$ for sodium salt is 196 cm^{-1}, but is much lower in the series of lanthanide complexes (Table 5). Due to the above-mentioned rules, the obtained values of $\Delta v(COO^-)$ indicate the chelating, bridging and/or mixed chelating–bridging modes of the carboxylate groups in the investigated lanthanide(III) complexes (Scheme 1: mode b–h).

XPS spectroscopy

In order to determine electron redistribution between the acceptor and the donor related to complex formation, the XPS investigations were carried out. The indicator of these changes can be the difference in the binding energy (E_b) of C1s and O1s electrons. All changes in binding energies of the electrons C1s and O1s in complexes spectra are the evidence of electron density redistribution in the O–C–O moiety caused by the complexation of the metal ions through the oxygen atoms of ligand. The difference between the E_b C1s and O1s values of H$_3$bta and its complexes can be the parameter that characterizes interactions of the carboxylate group with metal ions. This paper presents the results of the XPS analyses, which

allowed to determine the binding energies (E_b) for the main lines of C1s, O1s of H$_3$bta as well as Ln3d, Ln4d, Ln5p, spin–orbital splitting and full width at half maximum (FWHM) [35] for lanthanide(III) complexes. The XPS data are listed in Tables 6–8. Figure 7 shows high-resolution XPS spectra of H$_3$bta and lanthanide(III) complexes, and Fig. 8 shows deconvolution of only C1s and O1s spectra for H$_3$bta and the exemplary Eu(bta)·4H$_2$O complex. The deconvolution of the C1s spectrum of H$_3$bta shows three peaks, each of them belongs to carbon atoms in different surrounding [36]. The most intense component with the lowest binding energy (284.7 eV) corresponds to aromatic carbon atoms of benzene ring, and its position is stable in the spectra of acid and all lanthanide(III) complexes. The second peak (286.1 eV) corresponds to carbons from the methylene groups being a link between the aromatic ring and the –COOH groups. The band with the highest energy of 289.2 eV corresponds to carbon atoms from the carboxylic groups of acid. There is no satellite peak associated with the shake-up effect.

Table 6 and Fig. 8 demonstrate that position of E_b (C–C) lines is stable in all spectra; the binding energies for electrons in the CH$_2$ group in the complexes compared with that in H$_3$bta are the same for the Nd(III), Tb(III), Ho(III) complexes and different for Eu(III) ($\Delta E_1 = 0.2$ eV); and for La(III), Tm(III) and Lu(III) they cannot be extracted from C1s line. The main changes take place in the surrounding of carbon atoms which belong to the carboxylic groups. The binding energy of C1s decreases for the electrons in the O–C–O group in the complexes as compared to the O=C–O group in H$_3$bta, in the range $\Delta E_1 = 0.3$–0.5 eV. The change

Table 4 Vibrational frequencies (4000–400 cm^{-1}) and assignments of bands occurring in the IR spectra of H$_3$bta and its Na and Ln(III) compounds

Unscaled	Scales	H$_3$bta	Na	La	Nd	Eu	Tb	Ho	Tm	Lu	Assignments
3758	3600	3500–2500	3700–2700	3700–2700	3700–2700	3700–2700	3700–2700	3700–2700	3700–2700	3700–2700	$\nu(OH)_C + \nu(OH)_W$[a]
3757	3599										
3754	3596										
3173	3040	3072	3062	3038	3019	3073	3081	3091	3089	3056	$\nu(C_{ar}\text{–}H)$
3163	3030	3032	3020	3023	3008	3008	3008	3012	3027	3015	
3160	3027										
3123	2992	2972	2948	2970	2920	2928	2975	2931	2959	2964	$\nu_{as}(CH_2)$
3092	2962										
3089	2959										
3070	2940	2924	2912	2920	2896	2896	2896	2896	2920	2912	$\nu_s(CH_2)$
3037	2909										
3032	2905										
1819	1743	1723									$\nu(C{=}O)$
1817	1741	1705									
1809	1733	1693									
1648	1620	1605	1653	1656	1612	1612	1612	1601	1638	1578	$\nu(C_{ar}\text{–}C_{ar}) + \delta_s(OH)_W$[a]
1642	1614	1540	1606		1552	1548	1560	1543	1610	1564	
			1580	1540	1536	1536	1540	1564	1548	1552	$\nu_{as}(COO^-)$[a]
1495	1470										$\beta(C_{ar}\text{–}H) + \alpha(CCC)$
1492	1467	1461	1458	1457	1460	1454	1457	1460	1440	1443	$\nu(C_{ar}\text{–}C_{ar}) + \beta(C_{ar}\text{–}H)$
1482	1457	1414									$\beta(COH)$
1461	1436			1440	1439	1439	1439	1437			$\delta(CH_2)$
1460	1435										
1386	1362	1385									$\tau(H_{CH2}\text{–}C_{CH2}\text{–}C_C\text{–}O_C) + \nu(C_{CH2}\text{–}C_C) + \nu(C_{ar}\text{–}C_{CH2})$
1382	1358	1353									$\tau(HCCO) + \nu(C_{CH2}\text{–}C_C) + \beta(COH) + \nu(C\text{–}O)$
1360	1337										$\beta(COH) + \beta(H_{CH2}\text{–}C_{CH2}\text{–}C_C) + \nu(C\text{–}O) + \nu(C_{CH2}\text{–}C_C)$
			1384	1416	1432	1436	1436	1432	1432	1432	$\nu_s(COO^-)$[a]
				1396	1412	1412	1412	1412	1400	1400	
1345	1322		1332	1326	1364	1364	1364	1364	1333		$\beta(C_{ar}\text{–}H) + \nu(C_{ar}C_{ar})$
1329	1306	1313	1300	1300	1304	1304	1308	1308	1304	1300	$\nu(C_{ar}\text{–}C_{CH2}) + \beta(COH)$
1326	1303	1296	1280	1272	1280	1280	1280	1280	1284	1276	$\beta(C_{ar}\text{–}H)$
1309	1287	1266	1256	1248	1260	1264	1264	1264	1272		$\omega(CH_2)$

Table 4 continued

Unscaled	Scales	H₃bta	Na	La	Nd	Eu	Tb	Ho	Tm	Lu	Assignments
1295	1273										$\beta(COH) + \tau(HCCO)$
1279	1257										$\beta(COH) + \tau(HCCO) + \nu(C_{ar}C_{ar}) + \nu(C_{ar}-C_{CH2}) + \nu(C-OH)$
		1229									
1236	1215										$\beta(COH) + \beta(HCC_C)$
1215	1194	1193	1200	1188	1188	1188	1188	1192	1191	1194	$t(CH_2)$
1208	1187		1192								
1191	1171	1176	1176	1172	1164				1172	1172	$\beta(C_{ar}-H) + \nu(C_{ar}-C_{CH2}) + \alpha(CCC)$
1188	1168	1150									$\beta(C_{ar}-H) + \nu(C_{ar}-C_{CH2})$
1136	1117										$\nu(C-O) + \beta(COH)$
1131	1112										$\nu(C-O) + \beta(COH)$
1124	1105										$\nu(C-O) + \beta(HCC) + \tau(HCCO) + \beta(COH)$
1018	1001	1000	1004	1000	1000	1000	1000	1000	1004	1000	$\alpha(CCC) + \nu(C_{ar}C_{ar})$
1011	994		992	964	960	960	960	960	956	956	$\nu(C_{ar}-C_{CH2}) + \nu(C_{ar}-C_{ar})$
999	982										
966	950	960	956	944	948	949		944	944		$\tau(HCCO)$
938	922	920	936		940						
935	919										$\gamma(C_{ar}-H)$
		907									$\gamma(COH)$
929	913		928	924	932	932	932	924	920	924	$\gamma(C_{ar}-H)$
915	899		912	907	900	900	912	900			
909	894		888	880	885		900				
876	861	855	868	875	872	872	872	872		864	$\beta(COO^-)^a$
866	851										$\gamma(C_{ar}-H) + \nu(C_{CH2}-C_C) + \nu(C-O)$
											$\nu(C_{CH2}-C_C)$
844	830	798	784	782	786	756	758	758			$\nu(C_{CH2}-C_C) + \gamma(C_{ar}-H)$
797	783	728									$\pi(O-C-O-C) + \beta(C_{ar}-C_{CH2}-C_C) + \nu(CCH_2-C_C)$
743	730		736	744	744	744	744	744	744	748	$\gamma(COO^-)^a$
723	711										$\nu(C-O) + \tau(O-C-O-C)$
680	668		676	688	688	688	688	688	692	692	$\varphi(CCC) + \alpha(CCC)$
656	645	634	624	624	624	624	624	620	624	624	$\varphi(CCC) + \alpha(CCC) + \gamma(COH)$
652	641	607									$\gamma(COH)$
635	624										
615	604										$\beta(O=C-O)$

Table 4 continued

Unscaled	Scales	H_3bta	Na	La	Nd	Eu	Tb	Ho	Tm	Lu	Assignments
592	582		588	584	584	588	588	592	588	584	$\beta(O{=}C{-}O) + \beta_{as}(COO^-)$[a]
586	576										$\beta(O{=}C{-}O)$
542	533		556	559		560		560	555	576	$\pi(O{-}C{-}O{-}C)$
539	530										$\tau(CCCC_{CH2}) + \gamma(COH) + \varphi(CCC)$
514	505										$\gamma(COH)$
509	500										$\alpha(CCC) + \nu(C_{ar}{-}C_{CH2})$
486	478										$\beta(C_{ar}{-}C_{ar}{-}C_{CH2}) + \tau(H_{CH2}{-}C_{CH2}{-}C_{C}{-}O)$
445	437		412	404	408	412	416	416	404	404	$M{-}O$[a]

ν_{as}–ν_s, asymmetric–symmetric stretching; β, in-plane deformation; γ, out-of-plane deformation; plane and out-of-plane deformation for CH_2 groups: δ, scissoring; ρ, rocking; ω, wagging; t, twisting; $\alpha(CCC)$, in-plane deformation of aromatic system; $\varphi(CCC)$, out-of-plane deformation of aromatic system; τ, torsion; c, carboxylic; w, water; ar, aromatic
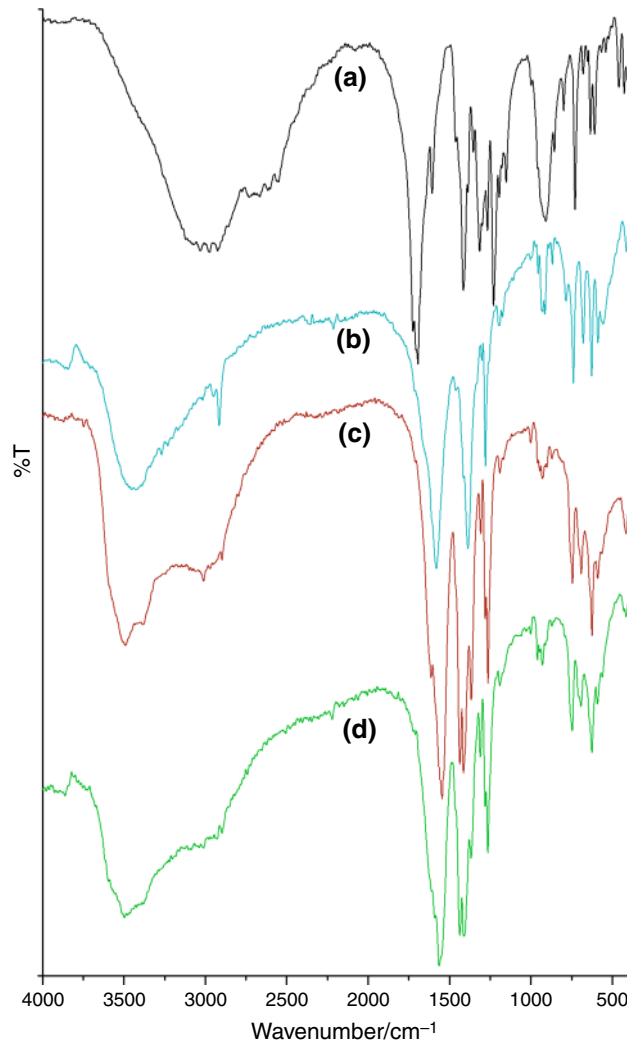
[a] Applies only to the complexes

Fig. 6 IR spectra of free H_3bta acid (**a**), its sodium salt (**b**) and its Ho(III) (**c**) and Tb(III) (**d**) complexes

Table 5 Stretching asymmetric $\nu_{as}(COO^-)$ and symmetric $\nu_s(COO^-)$ vibrational frequencies of carboxylate groups of bta ligand and the values of $\Delta\nu$ ($\Delta\nu = \nu_{as}(COO^-) - \nu_s(COO^-)$)

Compound	ν_{as} (COO⁻)	ν_s (COO⁻)	$\Delta\nu$
$Na_3(bta)\cdot2H_2O$	1580	1384	196
$La(bta)\cdot6H_2O$	1540	1416; 1396	124; 144
$Nd(bta)\cdot4H_2O$	1536	1432; 1412	104; 124
$Eu(bta)\cdot4H_2O$	1536	1436; 1412	100; 124
$Tb(bta)\cdot4H_2O$	1540	1432; 1412	108; 128
$Ho(bta)\cdot4H_2O$	1564	1432; 1412	132; 152
$Tm(bta)\cdot5H_2O$	1548	1432; 1400	116; 148
$Lu(bta)\cdot3H_2O$	1552	1432; 1400	120; 152

in the value of binding energy is an indicator of complex formation and an evidence of substantial variation of electron density in the carboxylate groups of different complexes.

Table 6 Binding energies E_b (eV) of C1s- and O1s lines for the H₃bta and its complexes

Compound	C1s (ΔE_1)[a]			O1s (ΔE_2)[b]	
	C–C/C–H	CH₂	O=C–O/O–C–O	C=O/C–O	O–H
H₃bta	284.7	286.1	289.2	532.3	533.6
La(bta)·6H₂O	284.7	–	288.8 (0.4)	531.9 (0.4)	533.6
Nd(bta)·4H₂O	284.7	286.1	288.8 (0.4)	531.9 (0.4)	533.5 (0.1)
Eu(bta)·4H₂O	284.7	286.3 (0.2)	288.7 (0.5)	531.8 (0.5)	533.3 (0.3)
Tb(bta)·4H₂O	284.7	286.1	288.9 (0.3)	532.0 (0.3)	533.4 (0.2)
Ho(bta)·4H₂O	284.7	286.1	288.9 (0.3)	532.1 (0.2)	533.6
Tm(bta)·5H₂O	284.7	–	288.7 (0.3)	531.9 (0.4)	533.4 (0.2)
Lu(bta)·3H₂O	284.7	–	288.8 (0.4)	532.0 (0.3)	–

[a] Difference in E_b between C1s in the H₃bta and in its complexes

[b] Difference in E_b between O1s in the H₃bta and in its complexes

Table 7 FWHM for the C1s and O1s lines for the H₃bta and Ln(III) complexes

Compound	C1s			O1s	
	C–C/C–H	CH₂	O=C–O/O–C–O	C=O/C–O	O–H
H₃bta	1.45	1.40	1.39	1.66	1.75
La(bta)·6H₂O	1.65	–	1.39	1.63	1.65
Nd(bta)·4H₂O	1.50	1.55	1.70	1.77	1.75
Eu(bta)·4H₂O	1.70	1.70	1.65	1.70	1.70
Tb(bta)·4H₂O	1.70	1.70	1.70	1.67	1.80
Ho(bta)·4H₂O	1.60	1.65	1.75	1.75	1.75
Tm(bta)·5H₂O	1.62	–	1.57	1.66	1.70
Lu(bta)·3H₂O	1.72	–	1.66	1.83	–

Table 8 Binding energies (E_b, eV) of 3d, 4p, 4d, 5p lines

Compound	E_b (eV)										
	3d₃/₂	3d₃/₂sat.	3d₅/₂	3d₅/₂sat.	4p₃/₂	4d₃/₂	4d₅/₂	5p₁/₂	ΔE_3^a	ΔE_4^b	ΔE_5^c
La(bta)·6H₂O	852.6	855.9	835.9	839.1	197	106	103	26	16.7	3.3,3.2	3
Nd(bta)·4H₂O	1006.1	–	983.5	–	229	121	–	19	22.6	–	–
Eu(bta)·4H₂O	1165.4	–	1135.8	–	262	143	137	20	29.6	–	6
Tb(bta)·4H₂O	1277.8	1284.5	1243.1	1252.3	–	151	–	25	34.7	6.7,9.2	–
Ho(bta)·4H₂O	–	–	–	–	–	164.5	162.3	30	–	–	2.2
Tm(bta)·5H₂O	–	–	–	–	333	177	175	33	–	–	2
Lu(bta)·3H₂O	–	–	–	–	359	207	197	34	–	–	10

[a] Difference in E_b 3d₃/₂–3d₅/₂

[b] Difference in E_b 3d_sat.–3d₃/₂, 3d_sat.–3d₅/₂

[c] Difference in E_b 4d₅/₂–4d₃/₂

Decrease of E_b means that the electron density on the atom increased upon complex formation. The deconvolution of the O1s spectrum of anhydrous H₃bta shows two peaks. Both peaks O1s belong to the carboxylic group. First (532.3 eV) belongs to the carbonyl (C=O) oxygen atom and the second one (533.6 eV) to hydroxyl (OH) oxygen atom from

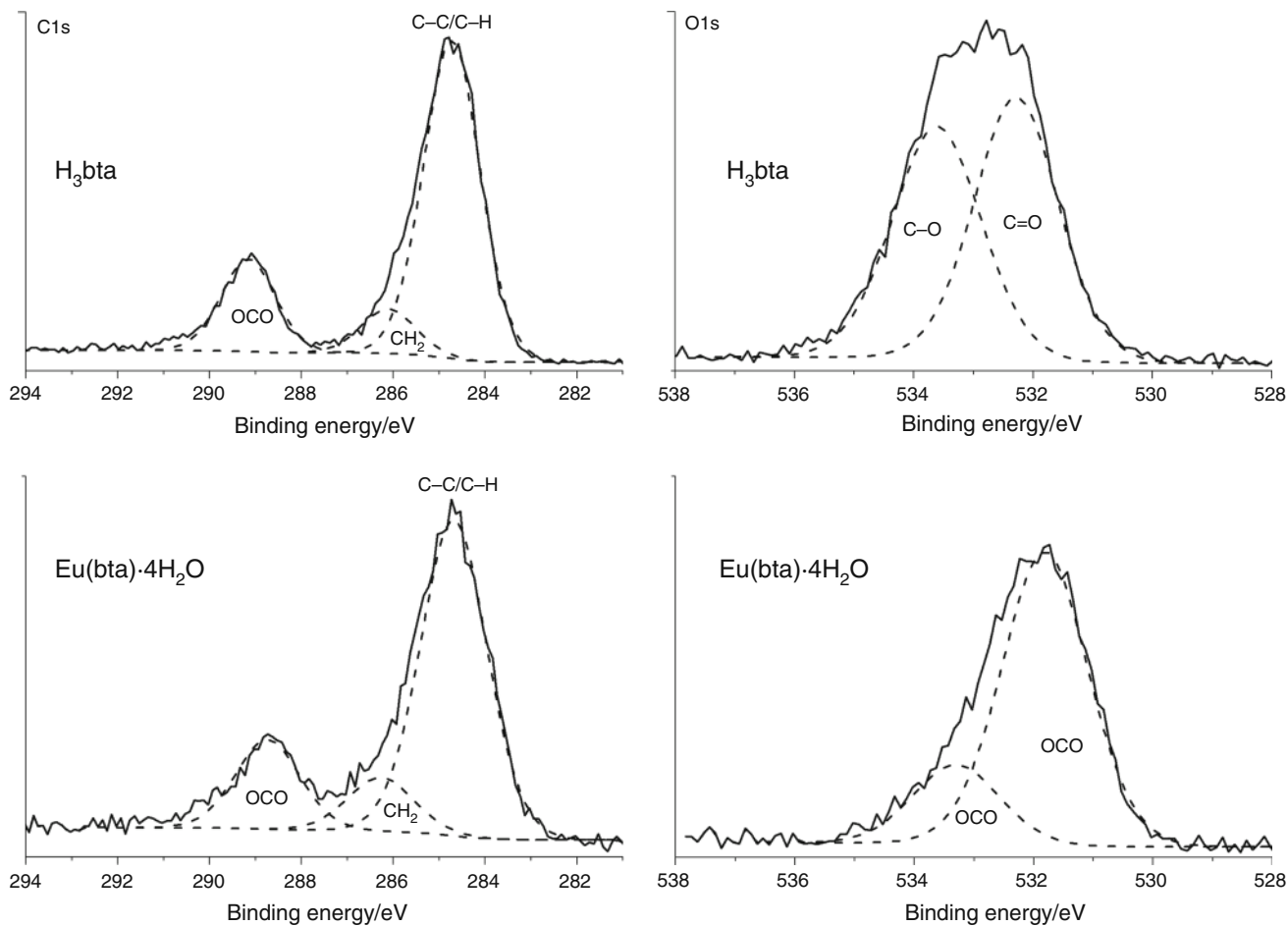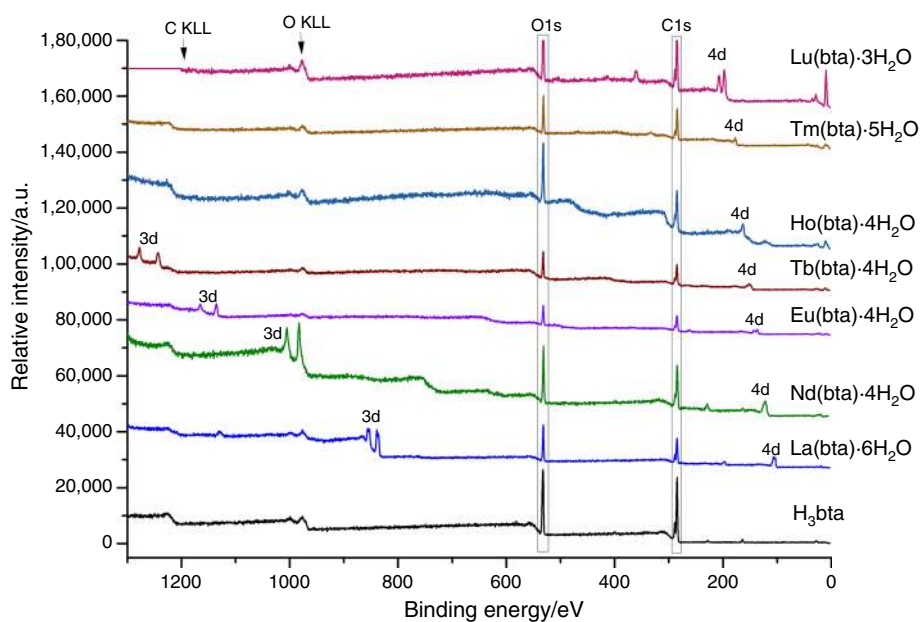Fig. 7 High-resolution XPS spectra of H_3bta and its complexes

Fig. 8 C1s and O1s spectra of H_3bta and Eu(bta)·4H_2O

carboxylic acid group. The formation of the complexes causes that energy binding of O1s electrons in the O–C–O groups of bta ligand becomes equal [36]. In the case of analysed complexes, one intensive line about 532 eV and the second one above 533 eV of low intensity can be observed instead of two intensive bands occurring in the spectrum of H_3bta (Fig. 8). This single intensive line located around 532 eV corresponds to one type of oxygen atoms, namely oxygen atoms forming carboxylate groups. The single line O1s is shifted towards smaller E_b values compared to acid spectrum, and the changes are in the range $\Delta E_2 = 0.2$–0.5 eV (Table 6). The FWHM of the O1s line is indicative of either one state of the O atom or insignificant difference of energy between two states, which makes them almost identical. The second peak of E_b equal 533.5 eV corresponds to the oxygen atom derived from water molecules [37]. All changes in binding energy C1s and O1s between H_3bta and complexes are the evidence of the redistribution of electron density in the O–C–O moiety caused by the complexation of the metal through the oxygen atoms. Figure 9 shows the deconvolution of La3d spectrum with four lines corresponding to spin–orbit splitting ($La3d_{3/2}$ and $La3d_{5/2}$) and their shake-up satellites at higher binding energy side. The energy separation between main lines ΔE_3 ($3d_{3/2}$–$3d_{5/2}$) and the satellite lines ΔE_4 ($3d_{sat.}$–$3d_{3/2}$ and $3d_{sat.}$–$3d_{5/2}$) is 16.7, 3.3 and 3.2 eV, respectively. Satellites are assigned to charge-transfer shake-up from ligand to empty 4f orbital [38–41]. One peak corresponds to the final state without the charge transfer $4f^0$, and the satellite peak corresponds to the final state after transfer of electron ($4f^1$) from ligand to 4f orbital of Ln(III). In Tb(III) complex, spin–orbit splitting ($3d_{3/2}$ and $3d_{5/2}$) and satellites are also observed. Energy separation between the main lines ΔE_3 and the satellite lines ΔE_4 is 34.7, 6.7 and 9.2 eV, respectively. The values ΔE_4 are different; in the case of La(III)
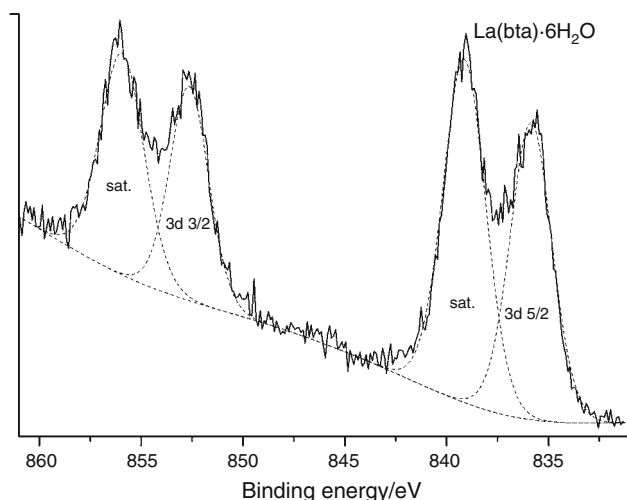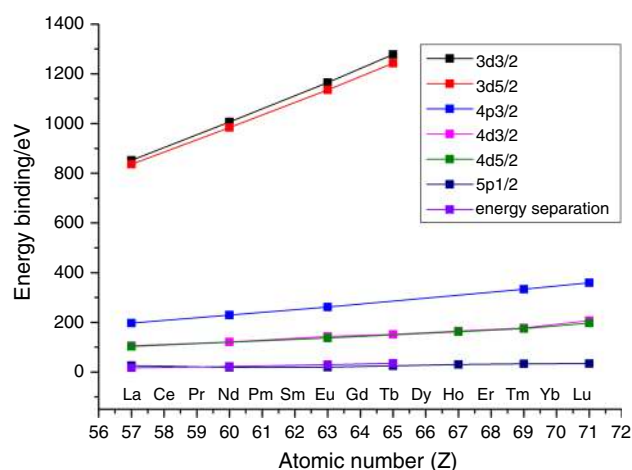

Fig. 10 Energy binding of 3d, 4p, 4d, 5p XPS lines and energy separation of 3d lines as a function of atomic number Z

compound, there is a small difference, but for Tb(III) complex it is larger. In the case of Nd(III) and Eu(III) complexes, only spin–orbit splitting lines are observed. An increase in the atomic number is accompanied by an increase in the binding energy 3d, 4d, 5p, and separation energy is shown in Fig. 10. All data are summarized in Table 8.

Conclusions

The obtained lanthanide(III) complexes of the formula $LnC_9H_9(COO)_3 \cdot 3$–$6H_2O$, where Ln = La(III), Nd(III), Eu(III), Tb(III), Ho(III), Tm(III) and Lu(III), are crystalline powders crystallizing in the monoclinic or triclinic crystal system. The complexes are stable under normal conditions, and removal of all water molecules does not lead to framework collapse. When heated, they decompose up to about 160–200 °C in two stages to stable anhydrous complexes. This indicates that in the structure of complexes there are hydrogen- and coordination-bonded water molecules. The values of dehydration energy increase with the increasing of atomic number of Ln(III) from 28 to 35 kJ mol^{-1} H_2O. The XRPD investigations of the compounds indicate that the framework and crystalline order are maintained despite removal of water molecules. The framework of anhydrous Ln(bta) is highly stable, but heated above 300–350 °C undergoes decomposition to Ln_2O_3 or Tb_4O_7. On the basis of IR spectra, the different ways of metal ions coordination through carboxylate oxygen atoms are possible: chelating, bridging and/or bridging–chelating. The XPS electronic spectra confirmed the deprotonation of carboxylic groups of H_3bta and their full transformation into carboxylate systems during complexes formation. The XPS study also revealed that in the structure of analysed complexes water molecules are present.

Fig. 9 3d XPS spectrum of La(bta)·6H₂O

References

1. Rao CNR, Natarajan S, Vaidhyanathan R. Metal carboxylates with open architectures. Angew Chem Int Ed. 2004;43:1466–96.
2. Rao CNR. Chemistry of materials. A letter to a young friend. Resonance. 2009;14:508–17.
3. Allendorf MD, Bauer CA, Bhakta RK, Houk RJT. Luminescent metal–organic frameworks. Chem Soc Rev. 2009;38:1330–52.
4. Parra DF, Forster PL, Łyszczek R, Ostasz A, Lugao AB, Rzączyńska Z. Thermal behavior of the highly luminescent poly(3-hydroxybutyrate): Eu(tta)$_3$(H$_2$O)$_2$ red-emissive complex. J Therm Anal Calorim. 2013;114:1049–56.
5. Łyszczek R. Hydrothermal synthesis, thermal and luminescent investigations of lanthanide(III) coordination polymers based on the 4,4′-oxybis(benzoate) ligand. J Therm Anal Calorim. 2012;108:1101–10.
6. Łyszczek R, Ostasz A, Bartyzel A, Lipke A. Thermal, spectroscopic and luminescence investigations of lanthanide(III) coordination polymers based on V-shaped 4,4′-sulfonyldibenzoic acid. J Anal Appl Pyrolysis. 2015;115:370–8.
7. Kurmoo M. Magnetic metal–organic frameworks. Chem Soc Rev. 2009;38:1353–79.
8. Li M, Liu B, Wang B, Wang Z, Gao S, Kurmoo M. Erbium-formate frameworks templated by diammonium cations: syntheses, structures, structural transition and magnetic properties. Dalton Trans. 2011;40:6038–46.
9. Hawes CS, Chilton NF, Moubaraki B, Knowles GP, Chaffee AL, Murray KS, Batten SR, Turner DN. Coordination polymers from a highly flexible alkyldiamine-derived ligand: structure, magnetism and gas adsorption studies. Dalton Trans. 2015;44:17494–507.
10. Wang LL, Luo F, Dang LL, Li JQ, Wu XL, Liu SJ, Luo MB. Ultrafast high-performance extraction of uranium from seawater without pretreatment using an acylamide- and carboxyl-functionalized metal–organic framework. J Mater Chem A. 2015;3:13724–30.
11. Jin HG, Yan YZ, Li J, Gu ZG, Chen JH, Liu YT, Zheng ZP, Zhan QG, Cai YP. 1-D to 3-D lanthanide coordination polymers constructed from 5-aminoisophthalic acid and oxalic acid. Inorg Chem Commun. 2012;23:25–30.
12. Liu K, You H, Jia G, Zheng Y, Song Y, Yang M, Huang Y, Zhang H. Coordination-induced formation of one-dimensional nanostructures of europium benzene-1,3,5-tricarboxylate and its solid-state thermal transformation. Cryst Growth Des. 2009;9:3519–24.
13. Rzączyńska Z, Ostasz A, Sikorska-Iwan M, Głuchowska H, Olszewska E, Pikus S. Synthesis and characterization of metal polycarboxylates constructed from lanthanides(III) and 1,2,4,5-benzenetetracarboxylic acid. J Therm Anal Calorim. 2006;84:575–9.
14. Ostasz A, Łyszczek R, Mazur L, Sienkiewicz-Gromiuk J, Rusinek I, Rzączyńska Z. Some properties of Nd and Er complexes with 1,2,3,4,5,6-benzeneheksacarboxylic (mellitic) acid. J Anal Appl Pyrolysis. 2013;99:203–10.
15. Li X, Wang C, Zheng X, Zou Y. Hydrothermal synthesis and crystal structure of two new lanthanide coordination polymers with 1,2-phenylenediacetate. J Coord Chem. 2008;61:1127–36.
16. Ren YX, Zhang ML, Li DS, Fu F, Wang JJ, Du M, Hou XY, Wu YP. Unusual (4,6)-connected lanthanide 1,3-phenylenediacetate coordination frameworks displaying lanthanide contraction effect and 1D and 2D mixed self-weaving architecture. Inorg Chem Commun. 2011;14:231–4.
17. Rusinek I, Sienkiewicz-Gromiuk J, Mazur L, Rzączyńska Z. Lanthanide(III) 1,4-phenylenediacetate complexes: the relation between the structure and thermal properties. J Inorg Organomet Polym. 2013;23:1068–77.
18. Zhang ZH, Shen ZL, Okamura T, Zhu HF, Sun WY, Ueyama N. Synthesis and structures of two series of coordination frameworks based on the assembly of 1,3,5-benzenetriacetic acid with lanthanide metal salts. Cryst Growth Des. 2005;5:1191–7.
19. Zhang ZH, Liu GX, Okamura T, Sun WY, Ueyama N. Synthesis, structures, and magnetic properties of new rare earth coordination polymers constructed by 1,3,5-benzenetriacetic acid. Struct Chem. 2006;17:3–11.
20. Zhang ZH, Meng WL, Okamura TA, Kong LY, Sun WY, Ueyama N. Lanthanide-organic framework with flexible triacid ligand: structural variation under different reaction conditions. Supramol Chem. 2006;18:317–25.
21. Zhang ZH, Okamura T, Hasegawa Y, Kawaguchi H, Kong LY, Sun WY, Ueyama N. Syntheses, structures, and luminescent and magnetic properties of novel three-dimensional lanthanide complexes with 1,3,5-benzenetriacetate. Inorg Chem. 2005;44:6219–27.
22. Huang YG, Jiang FL, Yuan DQ, Wu MY, Gao Q, Wei W, Hong MC. Intricate 3D lanthanide-organic frameworks with mixed nodes nets. J Solid State Chem. 2009;182:215–22.
23. Fitzgerald LJ, Gerkin RE. Interwoven hydrogen-bonding networks in benzene-1,3,5-triacetic acid. Acta Crystallogr C. 1997;53:967–9.
24. Frisch MJ, Trucks GW, Schlegel HB, Scuseria GE, Robb MA, Cheeseman JR, Scalmani G, Barone V, Mennucci B, Petersson GA, Nakatsuji H, Caricato M, Li X, Hratchian HP, Izmaylov AF, Bloino J, Zheng G, Sonnenberg JL, Hada M, Ehara M, Toyota K, Fukuda R, Hasegawa J, Ishida M, Nakajima T, Honda Y, Kitao O, Nakai H, Vreven T, Montgomery JA, Peralta JE, Ogliaro F, Bearpark M, Heyd JJ, Brothers E, Kudin KN, Staroverov VN, Kobayashi R, Normand J, Raghavachari K, Rendell A, Burant JC, Iyengar SS, Tomasi J, Cossi M, Rega N, Millam JM, Klene M, Knox JE, Cross JB, Bakken V, Adamo C, Jaramillo J, Gomperts R, Stratmann RE, Yazyev O, Austin AJ, Cammi R, Pomelli C, Ochterski JW, Martin RL, Morokuma K, Zakrzewski VG, Voth GA, Salvador P, Dannenberg JJ, Dapprich S, Daniels AD, Farkas O, Foresman JB, Ortiz JV, Cioslowski J, Fox DJ. Gaussian 03 W: Revision D.1. Gaussian Inc. Wallingford; 2005.
25. Cinar M, Karabacak M, Asiri AM. An experimental and density functional study on conformational and spectroscopic analysis of 5-methoxyindole-2-carboxylic acid. Spectrochim Acta A. 2015;137:670–6.
26. Jamróz MH. Vibrational energy distribution analysis: VEDA 4.0 program. Warsaw; 2004.
27. Silverstein R, Webster FX. Spectrometric identification of organic compounds. New York: Wiley; 1998.
28. Łyszczek R, Mazur L. Synthesis, crystal structure, spectroscopic and thermal investigations of neodymium(III) biphenyl-4,4′-dicarboxylate framework. Cent Eur J Chem. 2012;10:1165–74.
29. Kustaryono D, Kerbellec N, Calvez G, Freslon S, Daiguebonne C, Guillou O. New family of porous lanthanide-containing coordination polymers: [Ln$_2$(C$_2$O$_4$)$_3$(H$_2$O)$_6$, 12H$_2$O]$_\infty$ with Ln = La–Yb or Y. Cryst Growth Des. 2010;10:775–81.
30. Łyszczek R. Synthesis, structure, thermal and luminescent behaviors of lanthanide—pyridine-3,5-dicarboxylate frameworks series. Termochim Acta. 2010;509:120–7.

31. Rzączyńska Z, Kula A, Sienkiewicz-Gromiuk J, Szybiak A. Synthesis, spectroscopic and thermal studies of 2,3-napthalenedicarboxylates of rare earth elements. J Therm Anal Calorim. 2011;103:275–81.

32. Sienkiewicz-Gromiuk J, Rzączyńska Z. Structural, thermal, and spectra investigations of the lanthanide(III) biphenyl-4,4'-dicarboxylates. J Therm Anal Calorim. 2013;112:877–84.

33. Rzączyńska Z, Sienkiewicz-Gromiuk J, Głuchowska H. Structural and thermal properties of rare earth complexes with 2,2'-biphenyldicarboxylic acid. J Therm Anal Calorim. 2010;101:213–9.

34. Nakamoto K. Infrared and Raman spectra of inorganic coordination compounds. New York: Wiley; 1968.

35. Akitsu T, Einaga Y. Structures, magnetic properties and XPS of cyanide-bridged $Nd^{III}/Sm^{III}/Gd^{III}$–$Cr^{III}$ complexes. Inorg Chim Acta. 2006;359:1421–6.

36. Stevens JS, de Luca AC, Pelendritis M, Terenghi G, Downes S, Schroeder SLM. Quantitative analysis of complex amino acids and RGD peptides by X-ray photoelectron spectroscopy (XPS). Surf Interface Anal. 2013;45:1238–46.

37. Ivanova TM, Maslakov KI, Linko RV, Evstifeev IS, Kiskin MA, Shcherbakov IN, Savilov SV, Lunin VV, Novotortsev VM, Eremenko IL. XPS study of the electronic structure of heterometallic complexes $Fe_2MO(O_2CCH_3)_6(H_2O)_3]\cdot3H_2O$ (M = Co, Ni). Russ J Inorg Chem. 2014;59:670–7.

38. Ivanova TM, Kochur AG, Maslakov KI, Kiskin MA, Savilov SV, Lunin VV, Novotortsev VM, Eremenko IL. XPS study of the electron structure of heterometallic trinuclear complexes $Fe2M(\mu3\text{-}O)(\mu\text{-}Piv)6(HPiv)3$ (M = Mn Co, Ni). J Electron Spectrosc Relat Phenom. 2015;205:1–5.

39. Lixin Z, Bo W, Shiyan Y, Daosen J. XPS study of metal complexes with an unsymmetrical tridentate Schiff base. Polyhedron. 1993;12:1607–11.

40. Mullica DF, Lok CKC, Perkins HO, Benesh GA, Young V. The X-ray photoemission spectra of $Nd(OH)_3$, $Sm(OH)_3$, $Eu(OH)_3$ and $Gd(OH)_3$. J Electron Spectrosc Relat Phenom. 1995;71:1–20.

41. Ivanova TM, Shcherbakov IN, Linko RV, Kiskin MA, Evstifeev IS, Sidorov AA, Novotortsev VM, Eremenko IL. XPS study of the electronic structure of heterometallic complexes $Fe_2MO(Piv)_6(HPiv)_3$ (M = Ni, Co). Russ J Inorg Chem. 2013;58:945–50.